Higher viral virulence accelerates the evolution of host resistance

Carolin C. Wendling[1,2*], Janina Lange[1], Heiko Liesegang[3], Michael Sieber[4], Anja Pöhlein[3], Boyke Bunk[5], Jelena Rajkov[1,6], Henry Goehlich[1], Olivia Roth[1,6†], Michael A. Brockhurst[7†]

[1] GEOMAR Helmholtz Centre for Ocean Research Kiel, Marine Evolutionary Ecology, Düsternbrooker Weg 20, 24105 Kiel, Germany

[2] ETH Zürich, Institute of Integrative Biology, Universitätstrasse 16, CHN D 33, 8092 Zürich, Switzerland

[3] Georg-August-University Göttingen, department of genomic and applied microbiology, Grisebachstr 8 37077 Göttingen, Germany.

[4] Max Planck Institute for Evolutionary Biology, August-Thienemann-Str. 2, 24306 Plön, Germany

[5] Leibniz Institute DSMZ-German Collection of Microorganisms and Cell Cultures, Department Bioinformatics and Databases, Inhoffenstr. 7B, 38114 Braunschweig, Germany

[6] Kiel University, Marine Evolutionary Biology, Am Botanischen Garten 1-9, 24118 Kiel, Germany

[7] Division of Evolution and Genomic Sciences, University of Manchester, Dover Street, Manchester M13 9PT, UK

*Corresponding author:
E-mail: carolin.wendling@env.ethz.ch; Phone: +41 44 633 80 26

† shared last author

Abstract

Parasites and pathogens vary strikingly in their virulence and the resulting selection they impose on their hosts. While the evolution of different virulence levels is well studied, the evolution of host resistance in response to different virulence levels is less understood and as of now mainly based on theoretical predictions. Increased virulence can increase selection for host resistance evolution if resistance costs are outweighed by the benefits of avoiding infection. To test this, we experimentally evolved the bacterium *Vibrio alginolyticus* against two variants of the filamentous phage, VALGΦ8, that differ in their virulence. The bacterial host exhibited two alternative defence strategies against future viral infection: (1) super infection exclusion (SIE) whereby viral-infected cells were immune to subsequent infection at a cost of reduced growth, and (2) surface receptor mutations in genes encoding the MSHA type-IV pilus providing resistance to infection by preventing viral binding. While SIE emerged rapidly against both viruses, resistance evolved faster against the high virulence compared to the low virulence virus. Using a mathematical model of our system we show that increasing virulence strengthens selection for resistance due to the higher costs of infection suffered by SIE immune hosts. In both the experiments and the model, higher levels of evolved resistance in the host population drove more rapid virus extinction. Thus, by accelerating the evolution of host resistance, more virulent viruses caused shorter epidemics.

Keywords: virus, virulence, filamentous phages, experimental evolution, resistance evolution

INTRODUCTION

Infectious organisms vary strikingly in their level of virulence and the resulting selection they impose on hosts. Indeed, even closely related viruses, such as different strains of myxoma (1) or corona viruses (2), can differ greatly in virulence. While the evolution of virulence has been studied extensively during the last two decades, both using selection experiments (3-5) and observations of parasites evolved in nature (6, 7), how hosts respond to virulence-mediated selection is less well-explored. How virulence will impact evolutionary trajectories of resistance in a host population, and how these trajectories change with different levels of virulence, has been subjected to theoretical investigation. In general, increased virulence strengthens selection for the evolution of host resistance if the costs of resistance are outweighed by the benefits of avoiding infection (8-10). As such, at very low virulence, although infection is common, resistance is not favoured because the cost of resistance is likely to exceed any benefits of avoiding mild disease (9). With increasing virulence, resistance is more strongly selected as the cost of resistance becomes outweighed by the detrimental effects of more severe disease, leading to the more rapid evolution of resistance (10). However, at extremely levels of high virulence, selection for resistance can weaken once more, due to declining infection prevalence (8). Experimental tests of these predictions are, however, lacking.

To explore how viral virulence influences the dynamics of host resistance evolution, we designed a selection experiment using the model bacterium *Vibrio alginolyticus* K01M1 as a host and two variants of the filamentous phage, VALGΦ8, that differ in their virulence but are otherwise isogenic (Table 1). Filamentous phages (family *Inoviridae*)—i.e., long, thin proteinaceous filaments which contain a circular single-stranded DNA genome—have been shown to be ideal model systems to study virulence evolution (3, 5). Filamentous phages establish chronic infections whereby virions are continuously

81 released without lysis. Although filamentous phages do not kill their host, infections
82 cause harm by reducing host growth rates. This is because the host cell pays the metabolic
83 costs resulting from phage replication and from phage-encoded proteins inserted into the
84 bacterial membrane (11). Thus, virulence here is defined as the reduction in bacterial
85 growth resulting from phage infection, which can be directly quantified by measuring the
86 reduction in bacterial growth rate caused by phage infection relative to the growth rate of
87 phage-free cultures.

88 During chronic infections, most phage genes are repressed to ensure host cell
89 viability (12). This is achieved through the action of prophage encoded repressor proteins
90 whose actions also prevent superinfection (i.e., superinfection exclusion, SIE) by the
91 same (or closely related (13)) phage(s). In the case of filamentous phages, SIE immunity
92 is provided through the production of the phage-encoded receptor-binding protein pIII
93 which blocks primary and secondary phage receptors (11). Alternatively, it is possible for
94 bacteria to acquire resistance to filamentous phage infection through mutations causing
95 alterations to the surface receptors that the phages bind to, thus preventing phage infection
96 (15).

97 Combining experimental evolution with whole genome sequencing, we show that
98 SIE immunity arose rapidly and at a similar rate against both phages, whereas resistance
99 evolved more rapidly against the high compared to the low virulence phage, driving faster
100 extinction of the high virulence phage. Using an experimentally parameterised
101 mathematical model we show that accelerated replacement of SIE immunity by resistance
102 was driven by increasing costs of infection, in terms of reduced growth, suffered by SIE
103 immune hosts with increasing viral virulence. Resistance mutations were identified in
104 genes encoding the MSHA type IV pilus, which pleiotropically caused reduced motility
105 of these resistant bacteria. Together these data show that higher viral virulence accelerated

106 the evolution of resistance, which consequently drove faster virus extinctions and shorter
107 viral epidemics.

RESULTS AND DISCUSSION

Ecological dynamics vary according to phage virulence

To explore how variation in virulence influences the dynamics of host resistance evolution, we experimentally evolved the bacterium *Vibrio alginolyticus* K01M1 with or without one of two isogenic filamentous phages that differ in their virulence—VALGΦ8$_{K04M5}$ which reduces bacterial growth by 73% (higher virulence) or VALGΦ8$_{K04M1}$ which reduces bacterial growth by 58% (lower virulence, Table 1)—for 30 serial transfers (~240 bacterial generations). We first compared the ecological dynamics of bacterial and phage populations between treatments. Phages reduced bacterial densities by several orders of magnitude in both phage treatments compared to no phage control populations (Figure 1a). The immediate reduction (measured 24 hours post infection [hpi]) in bacterial density was greater in populations exposed to the higher virulence phage (VALGΦ8$_{K04M5}$) than the lower virulence phage (VALGΦ8$_{K04M1}$; Figure 1a). Correspondingly, in both treatments, phages amplified massively and rapidly, reaching 3.01×10^{12} PFU/ml (VALGΦ8$_{K04M5}$) 24 hpi and 2.83×10^{12} PFU/ml (VALGΦ8$_{K04M1}$) 48 hpi (Figure 1b), before declining to levels comparable to control populations (note that the genome of *V. alginolyticus* K01M1 contains a resident phage, VALGΦ6, that produces phage particles at a low background rate). These data suggest that the strong reduction in bacterial densities at the beginning of the experiment (Figure 1a) directly resulted from the costly production of viral particles (Figure 1b). Over time, however, the densities of bacterial populations exposed to the higher virulence phage recovered three times faster than populations exposed to the lower virulence phage (significant phage:transfer interaction in gls-model: $F_{15,186}=6.58$, $p<0.001$, Figure 1a). Bacterial population recovery was accompanied by declining phage densities in both treatments, but phage survival varied according to phage virulence (log-rank test:

133 $Chisq_1$=4.9, p=0.03), with the higher virulence phage going extinct more rapidly than the
134 lower virulence phage (Figure 4a).
135
136 **Rapid emergence of superinfection exclusion immunity**
137 These bacteria-phage population dynamics suggest that the emergence of bacterial
138 defences against phage infection may have enabled recovery of the host population.
139 Consistent with this hypothesis, the proportion of susceptible hosts rapidly declined to
140 zero within 24 hours in both treatments and remained so for the duration of the experiment
141 (Figure 1c). Bacteria can develop protection from filamentous phage infection by two
142 distinct mechanisms: superinfection exclusion (SIE) immunity, where already infected
143 cells are protected from subsequent infection by the same phage through phage-encoded
144 genes (14), or resistance, for instance via modification of the bacterial phage receptor,
145 preventing phage from entering the host cell (15). To quantify the frequency of SIE
146 immunity we used PCR with primers that target specifically VALGΦ8 to test for the
147 presence of the relevant phage in the bacterial genome (the presence of a PCR product
148 suggests SIE due to the presence of VALGΦ8 and those clones are from here on denoted
149 as Φ-carriers). SIE rapidly increased in frequency and dominated bacterial populations in
150 both treatments after 24 hours (Figure 1d). However, after 48 hours, the proportion of SIE
151 hosts began to decline, and did so significantly faster in populations that had been exposed
152 to the higher virulence phage (Figure 1d, significant phage:transfer interaction in glm:
153 $F_{6,60}$=10.18, p<0.001). Given that these populations contained no susceptible bacteria
154 from 24 hours onwards (out of 24 tested colonies per timepoint), the subsequent decline
155 of SIE hosts suggests their displacement by the invasion of resistant genotypes, and that
156 this was more strongly selected for by the higher virulence phage.

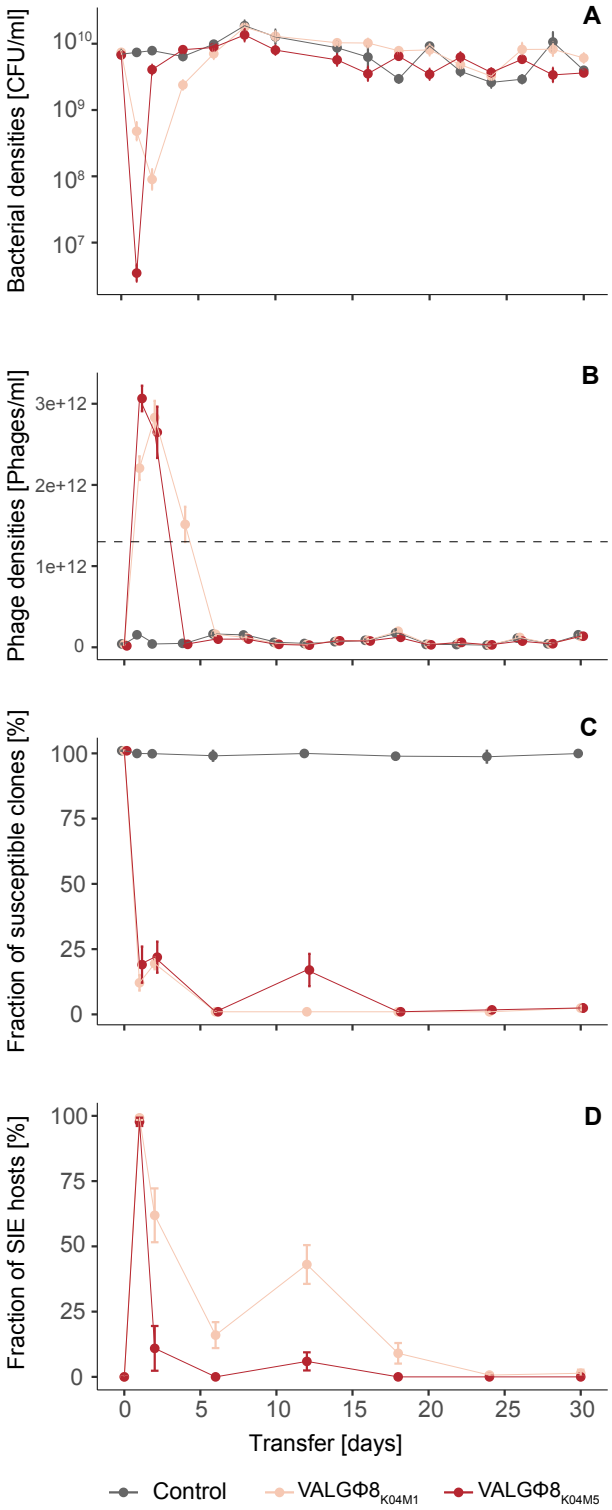

Figure 1 Population dynamics over 30 transfers. (A) Bacteria in CFU/ml, (B) Phages in PFU/ml, the grey dashed line represents the quantification limit below which quantifying filamentous phages using spectrophotometry is inaccurate, note: free phages in the control treatment stem from the low-replicating resident phage VALGΦ6 (see Table 1) (c) Fraction of susceptible clones (n=24), and (d) Fraction of SIE hosts within phage-resistant clones. Fractions are based on 24 random clones per replicate population per timepoint. In all panels, data are represented as mean of six replicate populations per treatments, error bars represent standard errors. Colours correspond to one of three experimental treatments, lower virulence VALGΦ8$_{K04M1}$ (light red), higher virulence VALGΦ8$_{K04M5}$ (dark red), no phage (grey).

166 **Resistance is associated with mutations in MSHA type IV pilus encoding genes**

167 To test if the decline of SIE hosts after 24 hours was driven by the invasion of surface
168 receptor modification resistance, we used whole genome sequencing (WGS) of two
169 randomly chosen clones from each population isolated at transfer 2: one PCR-positive
170 clone (Φ-carrier; resistance through superinfection exclusion) and one PCR-negative
171 clone (resistant but not phage carrying) to identify mutations. We observed no loci with
172 mutations on chromosome 2 or the plasmid pl9064, but on chromosome 1 we identified
173 12 loci with mutations that were not present in clones from the control treatment,
174 suggesting that these were associated with phage-mediated selection. Of these 12 loci,
175 three were randomly distributed across PCR-positive and PCR-negative clones. This
176 included an intergenic region between tRNA-Val and the 23S ribosomal RNA, that has
177 been repeatedly hit in both clone-types and phage-treatments, but whose function we
178 cannot explain. The remaining nine loci were exclusive to PCR-negative clones
179 suggesting a potential role in evolved phage resistance. Of these nine loci, eight had
180 substitutions, duplications, insertions, or deletions in four different genes belonging to the
181 MSHA type IV pilus operon (*mshL, mshE, mshG, K01M1_28150;* Figure 2a/ Table S1).
182 Among those, three caused severe frameshift mutations that presumably have a high
183 impact on the function of these proteins. While one locus (*K01M1_28150*) was affected
184 twice in both phage treatments, all other loci were treatment specific with mutations in
185 *mshL* and *mshE* being exclusively found against the higher virulence phage and in *mshG*
186 against the lower virulence phage. Moreover, we found more mutated MSHA-loci among
187 clones exposed to the higher virulence (5/6) compared to the lower virulence phage (3/6).
188 This supports of our previous findings, which suggested a stronger selection for resistance
189 against the higher virulence virus.

The absence of mutated MSHA-loci in PCR positive clones paired with a high prevalence in PCR-negative clones (8/12) suggests strongly parallel evolution of phage resistance. The MSHA operon is highly conserved across *Vibrio* clades (Figure 2b), and we found one corresponding ortholog to each gene in the *V. cholerae* El Tor MSHA operon (Figure 2b). This suggests that, similar to other vibrios (15), the MSHA type IV pilus plays an important role in resistance against the filamentous phage VALGΦ8. Note, a search of all assembled genomes for CRISPR associated genes as well as for CRISPR array like repetitive sequence patterns did not yield any results. All PCR-negative phage resistant clones are from here onwards referred to as Φ-resistant mutants. The genomic data also confirmed that clones with a positive PCR result (i.e., Φ-carrier) all contained the respective phage genome, which existed episomally in all sequenced clones (Table S2; Figures S3).

We found four PCR negative clones that were resistant to infections with ancestral phages but did not acquire mutations within the MSHA operon or other loci that might suggest a potential role in phage resistance. One explanation could be phenotypic resistance, where phage adsorption to bacteria is strongly reduced (16).

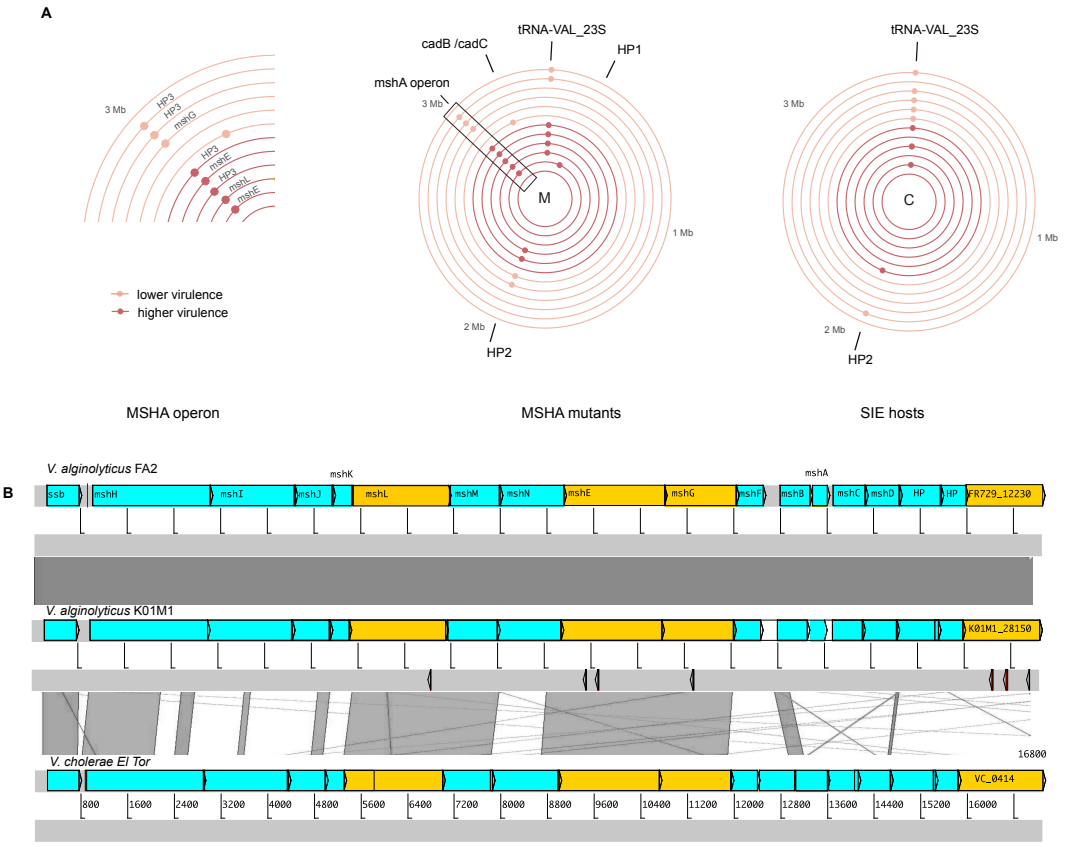

Figure 2 (A) Genetic loci on chromosome 1 under positive selection as indicated by parallel genomic evolution in populations exposed to phages: right: SIE hosts; middle: MSHA-mutants; left: zoom into MSHA-operon region from MSHA-mutants. Only loci which are not present in control populations are shown. Concentric circles correspond to one clone isolated from either the higher virulence VALGΦ8$_{K04M5}$ (six inner circles, dark red) or the lower virulence VALGΦ8$_{K04M1}$ phage (six outer circles, light red). Each coloured point corresponds to one mutation event on the respective clone. HP = hypothetical protein; HP3 corresponds to locus tag K01M1_28150. For more detailed information on the underlying mutation see Table S1.

(B) Structure of the MSHA-operon and comparative genomics comprising MSHA-operons from *V. alginolyticus* FA2 (top), *V. alginolyticus* K01M1 (middle), and *V. cholerae* El Tor (bottom). Similarity between regions is indicated by dark grey blocks, genes with detected mutations are marked in orange, detected mutations are marked as arrows below *V. alginolyticus* K01M1.

Virulence determines the rate of resistance evolution in a mathematical model

To generalize our findings across a wider range of virulence levels we developed an experimentally parameterized mathematical model. As in the experiment, bacterial densities dropped by several orders of magnitude upon phage infection (Figure 3a). By

simulating the infection dynamics over a wider range over virulence levels, we found that this drop occurred later and was less strong with decreasing virulence. While phage densities (irrespective of virulence) peaked 24 hpi, phages persisted longer and at higher levels when they were less virulent (Figure 3b). Similar to the experiment, the model predicts that SIE immunity emerges rapidly within 24 hpi (Figure 3c) but will only reach high levels if virulence is < 1. To capture the displacement of SIE hosts by MSHA-mutants we implemented a cost of reduced growth for SIE hosts which is directly linked to virulence (due to intracellular production of viral particles (Figure 4c)), i.e., the higher the virulence of the infecting phage, the lower the growth rate of the SIE host. MSHA-mutants grew at the same rate as the non-resistant clones (Figure 4e). We found that MSHA-mutants increased and replaced SIE hosts faster with increasing levels of virulence (Figure 3 c,d). Our model shows that this replacement occurs across a wide range of virulence levels, which we were not able to capture in the experiment. The faster replacement of SIE hosts by MSHA-mutants at higher virulence levels is driven by higher costs (i.e., reduced growth) of infection in SIE hosts, which increase monotonically with increasing phage virulence. Overall, our simulations predict that selection for resistance increases with virulence and that this is directly related to the costs of SIE, and thus resistance is more likely to evolve against higher virulence infections. This further suggests that to avoid extinction and enable long-term persistence in bacterial populations, filamentous phages should evolve towards lower virulence, reducing the cost of infection for SIE hosts and thus limiting selection for resistance.

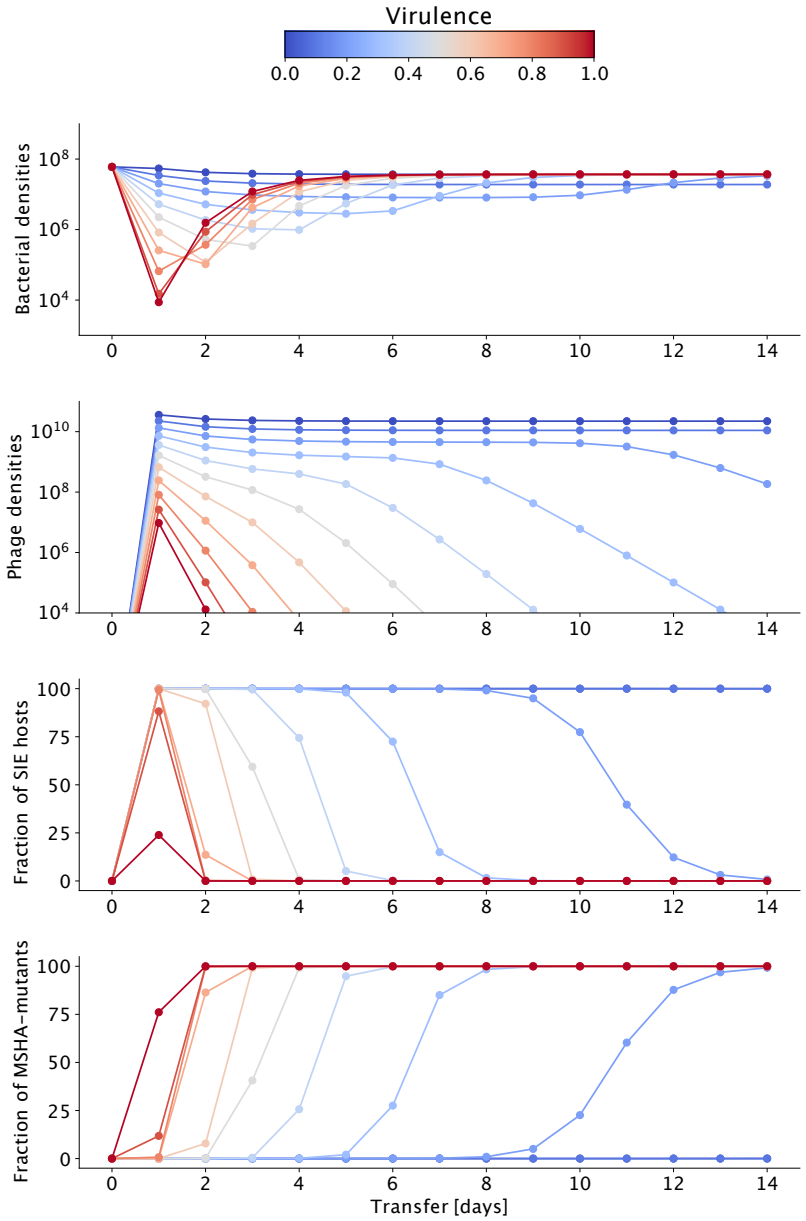

Figure 3: Results of model simulations of 14 transfers for (A) Bacteria in CFU/ml, (B) Phages in PFU/ml, (C) SIE hosts, and (D) MSHA-mutants depending on phage virulence (colour coded from blue: no virulence to red: high virulence).

Relative fitness of resistant mutants increases with phage virulence

To directly test our model predictions, that the fitness benefit of resistance relative to SIE immunity increases with increasing phage virulence, we performed a pairwise competition experiment, in which we quantified the relative fitness of MSHA-resistant mutants against SIE hosts (Figure 4b). The fitness benefit of the resistance mutation was

higher against bacteria carrying the higher virulence phage compared to bacteria carrying the lower virulence phage (significant treatment term in linear model with treatment, GFP-label and the interaction thereof as fixed factors: $F_{1,8}$=18.63, p=0.003, Table S3). These fitness data are consistent with the more rapid decline of VALGΦ8$_{K04M5}$-carriers than VALGΦ8$_{K04M1}$-carriers observed in the selection experiment and consistent with model predictions suggest stronger selection for resistance when exposed to a higher virulence phage. This explains the dynamics of the SIE hosts in the selection experiment, which went to extinction in five out of six populations exposed to the higher virulence phage 12 days post infection but were able to persist until the end of the experiment (i.e., transfer 30), albeit at very low frequencies, in five out of six populations exposed to the lower virulence phage.

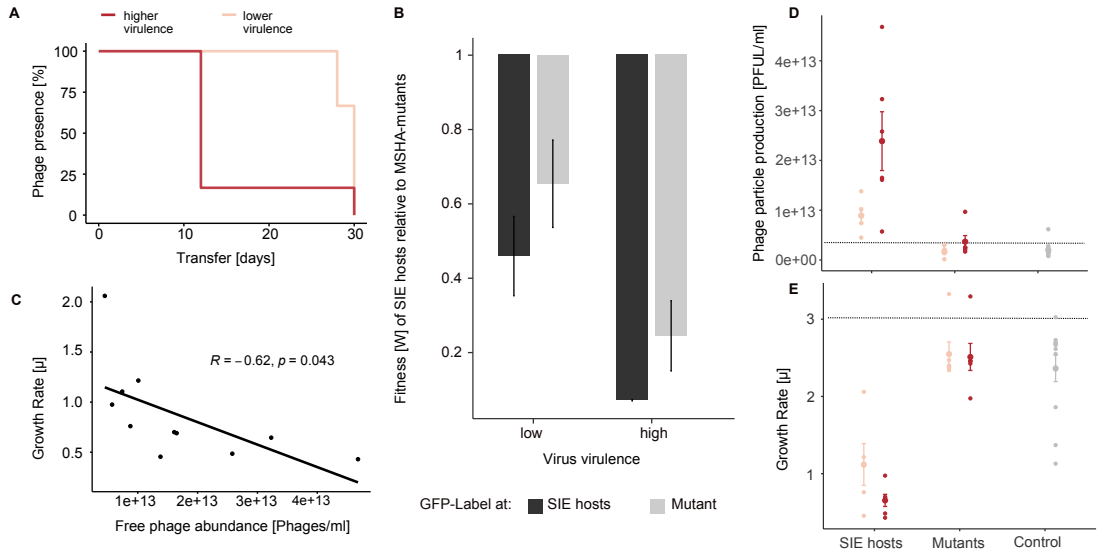

Figure 4 Phage prevalence (a) and fitness effects of evolved phage resistance versus immunity (b-e): (a) Phage prevalence for each co-evolving population in the presence of higher virulence phage VALGΦ8$_{K04M5}$ (dark red) or the lower virulence phage VALGΦ8$_{K04M1}$ (light red) over 30 transfers. (b) Darwinian fitness of SIE hosts relative to MSHA-mutants. A value of one corresponds to equal fitness. To account for potential costs associated with the GFP protein, competitions were performed where either the SIE hosts or the MSHA-mutants were labelled (n=3). (c) Correlation between bacterial growth rate [μ] and production of free phages measured as PFU/ml per clone. (d) Phage particle production [PFU/ml] and (e) Growth rate μ: both measured after 24 hours of bacterial growth for SIE hosts, MSHA-mutants, clones from the control populations (grey), and the ancestral K01M1 strain (horizontal line). Clones exposed to lower virulent VALGΦ8$_{K04M1}$ are shown in light red, clones exposed to higher virulent

VALGΦ8$_{K04M5}$ in dark red. Phages from the ancestral K01M1, from MSHA-mutants and the control clones stem from an ancestral filamentous *Vibrio* phage VALGΦ6 integrated on chromosome 2 of K01M1 (Table 1). Shown are means ± SEM, n=24.

Bacterial population densities during the selection experiment were negatively correlated with the number of SIE hosts per population (Pearson's correlation without zero inflation Φ-K04M1: r=0.69, t_{21}=-4.38, p<0.001, Φ-K04M5: r=0.92, t_7=-6.29, p<0.001; Figure S4). This implies that, even though the majority of the clones in the populations were protected from further infection, bacterial populations were unable to recover as long as the dominating mechanism of defence was SIE immunity, presumably due to virulence, resulting from the strong reduction in bacterial growth rate. To test this, we quantified differences in phage production and tested if phage production impaired bacterial growth in evolved clones. VALGΦ8$_{K04M5}$-carriers produced approximately 3.5 times more phage particles than VALGΦ8$_{K04M1}$-carriers (VALGΦ8$_{K04M5}$: mean = 2.39×10^{13} PFU/ml ± 1.44×10^{13}, VALGΦ8$_{K04M1}$: mean = 8.92×10^{12} PFU/ml ± 3.43×10^{12}, Figure 4d), and phage production significantly impaired bacterial growth (significant negative correlation between the amount of produced phages and bacterial growth rate, Figure 4c). Direct comparisons of growth rates among evolved clones showed that SIE hosts also grew slower than Φ-resistant mutants (VALGΦ8$_{K04M5}$: paired *t*-test: $t_{6.93}$=-9.69, p<0.001; VALGΦ8$_{K04M1}$: paired *t*-test: $t_{6.5}$=-4.58, p=0.003, Figure 4e). Together, these data suggest that SIE buys time, offering protection against subsequent infection, but at the cost of suffering the virulence of being infected. As in the model, where we predicted that the costs of SIE increase monotonically with phage virulence, SIE is eventually replaced by resistance, which happens faster with increasing levels of virulence, where the fitness benefits of resistance are greater. Ultimately dominance of host populations by resistant genotypes

resulted in faster extinction of higher virulence viruses, which were unable to overcome evolved host resistance.

Resistance leads to loss of motility

Many structures on the bacterial cell surface that serve as receptors for phages are multifunctional and phage resistance evolution through surface receptor modifications can come with secondary costs, for a review, see (17). In the case of bacterial appendages, such as flagella or pili, modifications often result in reduced motility and/or virulence during eukaryotic infections (18). We thus tested whether the observed mutations in the MSHA-pilus genes impair bacterial motility and observed reduced swimming motility of mutants compared to ancestral strains (Video Supplementary material). Since motility is an important fitness factor in the natural environment (18) we predict that the replacement of SIE by non-motile MSHA-mutants is constrained to laboratory environments, where such antagonistic pleiotropic costs of surface receptor modifications are lower than the costs of SIE. Selective pressures occurring in the natural environment, such as resource competition in eukaryotic hosts, might reverse this effect and explain why filamentous phages, including high virulent versions of VALGΦ8 persist in environmental isolates (19).

Concluding remarks

Filamentous phages are very common features of bacterial genomes (20), including those of environmental *Vibrio* strains closely related to our model strain K01M1, of which more than 50% are infected with the phage VALGΦ8 (19). While incorporating filamentous phage genomes into their own genome provides bacteria with immunity to future infection—through SIE immunity mediated by phage-encoded genes—we show

that this comes at a fitness cost that scales positively with the virulence of the phage. Higher phage virulence selects for the more rapid replacement of SIE immunity with resistance, causing phage extinction (Figure 4a). Thus, our data suggest, that to be able to establish long-term chronic infections, filamentous phages must either evolve very low levels of virulence (21), such that the resulting cost of virulence is outweighed by the cost of resistance mutations, or they must contribute positively to bacterial fitness by providing beneficial ecological functions (22). Those benefits may derive either from phage-encoded gene functions (e.g., toxins) (23-25), or from properties of the phage particles themselves (e.g., forming the biofilm extracellular-matrix (26), or acting as decoys for the vertebrate immune response (27)). Phage-mediated fitness benefits are often environmentally dependent (24, 28-30) and the prevalence of filamentous phages in bacterial genomes is higher in those isolated from eukaryotic infections (where filamentous phages often encode important enterotoxins) than those isolated from natural environments (11). Even though we have not yet identified its actual benefit, the high prevalence of VALGΦ8 in natural *V. alginolyticus* isolates (19) suggests that this phage provides a selective advantage outside the laboratory in its natural environment, i.e., the pipefish. Conversely, however, bacterial genomes are graveyards of defective prophages (31), including filamentous phages (32), suggesting that decay, rather than a peaceful coexistence, may be a common outcome for phages integrated into bacterial genomes. Ultimately, their level of virulence will dictate the fate of filamentous phages: Whereas lower virulence variants may enter into stable co-existence, higher virulence variants will be more prone to resistance-driven extinction and mutational decay if they do not provide a selective advantage.

MATERIAL AND METHODS

Experiments were conducted using the *Vibrio alginolyticus* strain K01M1 (33). K01M1 contains one integrated filamentous *Vibrio* phage VALGΦ6 (later called: resident K01M1Φ-phage throughout the manuscript), which replicates at a very low frequency (19). Compared to other, closely related *V. alginolyticus* strains, K01M1 is highly susceptible to infections by filamentous phages (14). For the selection experiment we used two different isogenic versions of the filamentous *Vibrio* phage VALGΦ8: VALGΦ8$_{K04M1}$ (lower virulence) and VALGΦ8$_{K04M5}$ (higher virulence; Table 1, for similarity between phages see Supplementary information and Figure S1), which have been isolated from two different hosts (*V. alginolyticus* K04M1 and *V. alginolyticus* K04M5). While both phages have been shown to significantly reduce the growth of K01M1 (14, 34), infections with the higher virulence VALGΦ8$_{K04M5}$ impose a significantly stronger reduction in bacterial growth than infections with the low virulence phage VALGΦ8$_{K04M1}$. All experiments were carried out in liquid medium (Medium101: 0.5% (w/v) peptone, 0.3% (w/v) meat extract, 3.0% (w/v) NaCl in MilliQ water) at 25° C in 30-ml microcosms containing 6 ml of medium with constant shaking at 180 rpm.

Table 1 Bacteria and phages (including NCBI accession numbers) used in the present study.

Isolate	Accession Number(s)	Phages	Role in evolution experiment
V. alginolyticus K01M1	CP017889.1 CP017890.1	*Vibrio* phage VALGΦ6	Host strain during evolution experiment
V. alginolyticus K04M1	CP017891.1 CP017892.1	*Vibrio* phage VALGΦ6 *Vibrio* phage VALGΦ8	Donor of the episomal, low virulence phage
V. alginolyticus K04M5	CP017899.1 CP017900.1	*Vibrio* phage VALGΦ6 *Vibrio* phage VALGΦ8	Donor of the integrative, high virulence phage
Vibrio phage VALGΦ6	MN690600		Resident phage in ancestral K01M1
Vibrio phage VALGΦ8	MN719123		Phage used in selection experiment

375 (a) Selection experiment

376 Six replicate populations were founded for each of three treatments from independent
377 clones of K01M1. Treatments comprised (a) the higher virulence VALGΦ8$_{K04M1}$, (b) the
378 lower virulence VALGΦ8$_{K04M5,}$ or (c) no phage as control. Each population was
379 established from 60 μl of an independent overnight culture (5×10^8 CFU/ml). At the
380 beginning of the experiment, we inoculated phage-containing treatments with 300 μl of a
381 5×10^{10} PFU/ml stock solution. Populations were propagated by transferring 0.1% to fresh
382 medium every 24 hours for a total of 30 transfers. On transfer T0, T1, T2 followed by
383 every other transfer, phage and bacterial densities were determined, as described below
384 and whole population samples were frozen at -80° C at a final concentration of 33%
385 glycerol. In addition, on transfer T0, T1, T2, T6, followed by every sixth transfer 24 single
386 colonies were isolated at random from each population and stored at -80° C. These
387 colonies were later used during follow-up assays, as described below. Two populations
388 from the control treatment tested positive for virus infection, indicating contamination,
389 were excluded from later assays.

390

391 (b) Bacterial and phage densities

392 *Bacterial densities*: bacterial densities were determined by plating out 100 μl of a
393 dilution series ranging from 10^{-5} to 10^{-7} on *Vibrio* selective Thiosulfate Citrate Bile
394 Sucrose Agar (TCBS) plates (Sigma Aldrich). Plates were incubated over night at 25° C
395 and the total amount of colonies was counted the following day.

396 *Phage densities*: quantification of filamentous phages by standard spot assays is often
397 not possible (Rakonjac 2011). Instead of typical lytic plaques we mostly observed opaque
398 zonas of reduced growth. Thus, we used spectrometry to quantify phage prevalence
399 (http://www.abdesignlabs.com/technical-resources/bacteriophage-spectrophotometry),

which uses the constant relationship between the length of viral DNA and the amount of the major coat protein VIII of filamentous phages, which, together, are the main contributors of the absorption spectrum in the UV range. The amount of phage particles per ml can be calculated according to the following formula:

$$\text{phages/ml} = \frac{(\text{OD269} - \text{OD320}) * 6e16}{\text{bp}},$$

where OD269 and OD320 stand for optical density at 269 and 320 nm and bp stands for number of base pairs per phage.

The method is based on small-scale precipitation of phages by single PEG-precipitation. After centrifuging 1500 μl of the phage containing overnight culture at 13,000 ×g for 2 min, 1200 μl of the supernatant was mixed with 300 μl PEG/NaCl 5× and incubated on ice for 30 min. Afterwards phage particles were pelleted by two rounds of centrifugation at 13,000 ×g for 2 min, resuspended in 120 μl TBS 1× and incubated on ice. After one hour the suspension was cleaned by centrifugation at 13,000 ×g for 1 min and absorbance was measured at 269 and 320 nm.

Quantification of filamentous phages using spectrometry is likely to be erroneous if viral load is low. Therefore, we additionally quantified phage prevalence/ phage extinction in each of the populations on every second transfer day by standard spot assays with a serial dilution (up to 10^{-6}) on the ancestral host (for details see (14)) and measured until which dilution the typical opaque zones of reduced bacterial growth were visible.

(c) Measuring phage-defence

We quantified the bacteria could not get infected by the respective ancestral phage by determining the reduction in bacterial growth rate (RBG) imposed by the phage, adapted from (35) with some modifications according to (36). Twenty-four random colonies from each population from transfer T0, T1, T2, T6, T12, T18, T24, and T30 were

introduced into 96-well microtiter plates containing Medium101 at a concentration of 5×10^6 cells/ml and inoculated with ~2.5×10^6 PFU/ml of the respective ancestral phage used for the selection experiment or without phage (control). Absorbance at 600 nm was measured using an automated plate reader (TECAN infinite M200) at T0 and again after 20 hours of static incubation at 25°C. The reduction in bacterial absorbance 'RBG' was calculated according to the following formula:

$$\mathrm{RBG} = \frac{\mathrm{OD600}(t=20) - \mathrm{OD600}(t=0)[\mathrm{Phage}]}{\mathrm{OD600}(t=20) - \mathrm{OD600}(t=0)[\mathrm{Control}]},$$

where OD stands for optical density at 600nm.

(d) Frequency of prophage carriage

On transfer T0, T1, T2, T6 followed by every sixth transfer we measured the frequency of phage carriage of 24 random clones per population using standard PCR. Primers (VALGΦ8_Forward TGGAAGTGCCAAGGTTTGGT, VALGΦ8_Revers GAAGACCAGGTGGCGGTAAA) that specifically target the *Vibrio* phage VALGΦ8 have been designed using NCBI Primer-BLAST webpage (httdol://www.ncbi.nlm.nih.gov/tools/primer-blast/). Glycerol stocks were inoculated overnight (25°C, 180 rpm) in Medium101 and subsequently diluted (1:10) in HPLC purified H_2O and frozen at -80° C. One μl of this suspension was used as DNA template in the PCR assay. Reaction comprised 1 μl Dream Tag Buffer, 0.1 μl Dream Tag DNA polymerase (Thermo Scientific, USA), 4.9 μl H_2O, 1 μl dNTPs [5 mM] and 1 μl of each primer [50 μM]. The amplification program used consisted of: (i) 3 min at 95° C, (ii) 35 cycles of 45 sec at 95° C, 30 sec at 63° C, 45 sec at 72° C, (iii) 7 min at 72° C. Afterwards, 5 μl of each reaction was mixed with 2 μl loading dye (10×) and loaded onto a 1.2% agarose gel dissolved in 1×TAE gel buffer. GeneRuler Express DNA-ladder was used as size marker. Agarose gels were run 15 min at 70 V in 0.5× TAE running buffer and

subsequently stained with ethidium bromide for 10 min. DNA was visualized using UV light and documentation took place using Intas Gel iX20 Imager. Phage presence was recorded positive if a PCR product of 1209 bp was visible.

For all subsequent assays, we randomly picked one immune clone with a positive PCR product (later called: Φ-carrier) and one resistant clone with a negative PCR product (later called: Φ-resistant mutant) from each phage-evolved population as well as two randomly selected non-resistant clones from the control populations.

(e) Competition experiments

To determine differences in fitness between both resistance forms, we measured the competitive fitness of three randomly selected Φ-carrier relative to three randomly selected Φ-resistant mutants from each treatment. Each competition culture was done in triplicates as described in (37). In brief, overnight cultures of both competing strains (of which one was labelled with a GFP-marker) were mixed 1:1 and 60 μl of this mixture was inoculated to 6 ml Medium 101 to initiate each competitive culture. After 24 hours, fitness was estimated by means of flow cytometry (FACS-Caliburm Becton & Dickinson, Heidelberg, GER), where absolute fluorescent cells and non-fluorescent cells were calculated. Competitive fitness was estimated as the ratio in Malthusian parameters (38):

$$W = \ln(abundance_{t=24}/abundance_{t=0})_{competitor1} / \ln(abundance_{t=24}/abundance_{t=0})_{competitor2}$$

(f) Bacterial growth rate and phage production

To determine fitness parameters that could explain observed differences in competitive fitness we additionally quantified bacterial growth rate (μ) by means of 24-hour growth curves and phage production using PEG precipitation (as described in (c)) of the same

clones used for the competition assays (i.e., one Φ-carrier and one Φ-resistant mutant from each phage-treated population and two random phage-susceptible clones from the control populations plus ancestors).

(g) Motility

Motility was visualized on mid-exponential growth cultures using a light microscope and swimming was captured for 50s.

(h) Whole genome sequencing

We used a combination of long- and short read sequencing to obtain complete genomes of the same clones from the assays above, i.e., one Φ-carrier and one Φ-resistant mutant from each phage-treated population and one random phage-susceptible clone from each control population, which corresponds to six independently evolved clones per treatment and resistance form. Clones were taken from timepoint 2, because phage-carriers disappeared quickly from the populations and we were thus not able to pick one mutant and one Φ-carrier from the same timepoint and population later than timepoint two. High molecular weight DNA was extracted from cell pellets of overnight cultures following the protocol for gram negative bacteria from the DNeasy Blood & Tissue Kit (Qiagen, Hilden, Germany). Long-read sequencing was performed at the Norwegian Sequencing Centre according to the following protocol: the library was prepared using Pacific Bioscience protocol for SMRTbell™ Libraries using PacBio® Barcoded Adapters for Multiplex SMRT® Sequencing. To do so, DNA was fragmented into 10kb fragments using g-tubes (Covaris). Samples were pooled during library preparation aiming for equimolar pooling and library size was selected using Ampure beads. The library was sequenced on a PacBio Sequel instrument using Sequel Polymerase v3.9, SMRT cells v3

LR and Sequencing chemistry v3.0. Loading was performed by diffusion. Two SMRT cells were sequenced (movie time: 600min, pre-extension time: 240 min). Reads were demultiplexed using Barcoding pipeline on SMRT Link (v6.0.0.47841, SMRT Link Analysis Services and GUI v6.0.0.47836) with 40 as a minimum barcode score.

For short read sequencing concentration and purity of the isolated DNA was first checked with a Nanodrop ND-1000 (PeqLab Erlangen, Germany) and exact concentration was determined using the Qubit® dsDNA HS Assay Kit as recommended by the manufacturer (Life Technologies GmbH, Darmstadt, Germany). Illumina shotgun libraries were prepared using the Nextera XT DNA Sample Preparation Kit. To assess quality and size of the libraries, samples were run on an Agilent Bioanalyzer 2100 using an Agilent High Sensitivity DNA Kit as recommended by the manufacturer (Agilent Technologies, Waldbronn, Germany). Concentration of the libraries were determined using the Qubit® dsDNA HS Assay Kit as recommended by the manufacturer (Life Technologies GmbH, Darmstadt, Germany). Sequencing was performed on a MiSeq system with the reagent kit v3 with 600 cycles (Illumina, San Diego, CA, USA) as recommended by the manufacturer and resulted in a minimum average coverage of 88× per strain (coverage range was from 88× to 157×). The reads were quality controlled using the program FastQC Version 0.11.5. All illumina reads that passed the FastQC filtering were used for hybrid assemblies as well as for single nucleotide variation analysis.

Genome assemblies were performed in two different ways: (i) long-read data was generated for all replicates where the presence of the infecting phage was confirmed by PCR. The Assemblies were performed as hybrid assemblies using short-read and long read data in a short-read first approach. In brief: An initial assembly was performed with short-read only using spades (v3.13.0) as provided within Unicycler (39). The resulting contigs were co-assembled with long-read data using miniasm (v0.2-r168) (40) and

curated using the racon software (41). This step resulted in complete closed replicons. All long reads were mapped and integrated into the contigs. All replicons were polished using Pilon (v1.22) to clear any small-scale assembly errors (42). Finally, all replicons were rearranged according to the origin of replication. (ii) the assembly for the ancestral K01M1 strain, as has been described in (14) was performed following the Hierarchical Genome Assembly Process (HGAP3) protocol, developed for Pacific Biosciences Single Molecule Real-Time (SMRT) sequencing data (43). HGAP is available for use within PacBio's Secondary Analysis Software SMRTPortal. Methodically, the longest subreads of a single SMRT Cell (usually 25x genome coverage, e.g., 25 x 5 Mbp = 125 Mbp) are being chosen to be error-corrected with "shorter" long reads in a process named preassembly. Hereby, a length cut-off is computed automatically separating the "longer" reads (for genome assembly) and the "shorter" reads (for error-correction). The level of error-correction is being estimated with a per-read accuracy of 99%. Finally, error-corrected long read data is being assembled with Celera Assembler (v7.0) (44).

(i) SNV analysis and reconstruction of infecting phages

All short-read sequences were mapped on a high quality closed reference genome of *Vibrio alginolyticus* Strain K01M1 (14) using Bowtie2 (45). Single nucleotide variation (SNV) analysis was done using the Breseq pipeline as described in (46). Whole genome alignments have been calculated using the MAUVE aligner (47). Presence of infecting phage genomes were confirmed by assembling NGS-reads that did not map on the K01M1 genome in a bowtie2 mapping using Spades (39). The resulting contigs were annotated based on the review of Mai-Prochnow on filamentous phages (11). The genomes of the evolved phages were compared to the infecting phage genomes *Vibrio* phage VALGΦ8 as well as to the genome of the resident prophage *Vibrio* phage

VALGΦ6 from the challenged strain K01M1 using BLAST and Easyfig 2.1 (48).

(j) Statistical analysis

All statistics were performed in the R 4.0.4 statistical environment (49). For all analysis aimed to compare the two different phage treatments to one another, control populations (i.e., those that evolved without phages) were excluded. When comparing temporal dynamics between phage-treatments, we excluded the starting time-point T0, because these measurements were taken before phages were added to the populations.

Bacteria and phage dynamics

Bacterial and phage densities were analysed over time using a generalized least squares model to control for autocorrelation of residuals over time using the gls function (package nlme) with phage treatment, transfer as categorical variable as well as their interaction as fixed effect.

We considered phages to be prevalent in the population if opaque zones of reduced growth were visible during standard spot assays. Phage prevalence was subsequently quantified by a serial dilution, which were assigned with invers values (i.e., if reduced growth zones were visible up to dilution of 10^{-6} we assigned to it a value of 7, whereas if they were only visible on an undiluted spot, we assigned to it a value of 1, if no zone of reduced growth was visible it was scored as 0). Phage extinction events across phage-treatments were analysed using a log-rank test.

Measuring phage defence and prevalence

We observed a bimodal histogram on all RBG values with a local minimum at RBG = 0.82 (Figure S2). Thus, we considered an infection as positive if RBG < 0.82. The

575 proportion of clones per population that could not get infected by the ancestral phage as
576 well as the proportion of clones that tested positive for PCR (targeting the VALGΦ8)
577 were analysed using a generalized linear model with a binomial error distribution using
578 the glm function (package lme4) with phage treatment, transfer and their interaction as
579 fixed effect.
580
581 *Fitness effects*
582 We determined differences in relative fitness between MSHA-mutants and SIE hosts
583 using a linear model with resistance mechanisms and GFP-label and the interaction
584 thereof as fixed effects. Maximum growth rates (μ) were estimated for each strain by
585 fitting generalized logistic models to individual growth curves using the open-source
586 software package Curveball (https://github.com/yoavram/curveball) (50) in python. To
587 determine differences in the amount of free phages and in growth rates produced
588 between ancestral strains and evolved strains and between both resistance forms, we
589 used Welch's pairwise *t*-tests with sequential Bonferroni correction. We further
590 performed a Pearson's correlation analysis to determine whether phage production
591 impacted bacterial growth rates.
592
593 (k) Mathematical model
594 We modelled the dynamics of the non-resistant evolved clones (with density B),
595 resistant SIE hosts (I), resistant MSHA-mutants (R), and SIE hosts that have also
596 acquired the MSHA mutation (IR), as well as the phage population (V) in batch cultures
597 by the following system of differential equations:
598 $$\frac{dB}{dt} = (1-m)g(B_{total})B - \phi BV$$

599 $$\frac{dI}{dt} = (1-m)(1-v)g(B_{total})I + \phi BV$$

600 $$\frac{dR}{dt} = (R + mB)g(B_{total})$$

601 $$\frac{dIR}{dt} = \big((1-v)IR + mI\big)g(B_{total})$$

602 $$\frac{dV}{dt} = ß(I + IR) - dV$$

603

604 Bacterial growth was modelled by generalized logistic growth of the form
605 $g(B_{total}) = r\left(1 - \left(\frac{B_{total}}{K}\right)^{w}\right)$. Here r is the maximum growth rate (mgr) of the non-
606 resistant evolved bacteria, K is the carrying capacity of the batch culture and $B_{total} =$
607 $B + I + R + IR$ is the total density of all bacterial types. The curvature parameter w
608 determines whether maximum growth is attained at an early point in the growth phase
609 ($w < 1$) or at a late point (w > 1). We assume that SIE hosts (I and IR) suffer a growth
610 rate reduction relative to the non-resistant evolved bacteria due to virulence caused by
611 intra-cellular production of virus particles, here represented by the virulence factor v <=
612 1. A completely avirulent virus would have v=0, and maximum virulence v=1
613 corresponds to growth arrest of the bacterial cell.

614 Viruses (*V*) infect non-resistant evolved bacteria (*B)* following a mass action law
615 with adsorption rate (phi), reflecting that increasing densities of either bacteria or viruses
616 lead to higher encounter rates and thus more infections. Infection of a bacterial cell
617 transforms cells into a resistant Φ-carrier (*I)*, which actively produces new viral particles
618 (*V*) with phage production rate (*ß*). Additionally, both non-resistant evolved bacteria (*B)*
619 and SIE hosts (*I)* can acquire complete resistance (*R* & *IR*) through mutations within the
620 MSHA type IV pilus operon. We assume that MSHA-mutants have the same growth
621 rate as the non-resistant evolved bacteria.

All bacterial types grow until the carrying capacity (K) is reached, but bacteria-virus interactions continue to occur as long as there are sensitive bacteria and viruses left. After a certain time t_{max} a portion (here 1/1000th) of the entire community is transferred to fresh medium and the process restarts.

Table 2 Parameter values of mathematical model and their biological meaning

Parameter	Biological meaning	Value
r	Maximum growth rate (mgr) of ancestor B	2.5 (h^{-1})
K	Carrying capacity of bacteria	10^9 cells/ml
w	Curvature parameter	0.02
v	Virulence	variable
phi	Phage adsorption rate	10^{-8} (h^{-1})
β	Phage production rate	50 (phages/cell h^{-1})
d	Phage decay rate	0.01 (h^{-1})
m	Mutation rate	10^{-8}

Acknowledgements: We thank Pratheeba Pandiaraj, Katja Trübenbach, Veronique Merten, Silke-Mareike Merten and Kim-Sara Wagner for their support in the laboratory.

Funding: This project received funding from three grants from the DFG [WE 5822/ 1-1], [WE 5822/ 1-2], and [OR 4628/ 4-2] within the priority programme SPP1819 given to CCW and OR and a DFG grant within the Cluster of Excellence 80 "The Future Ocean" given to CCW.

Data availability: All experimental data have been deposited on dryad (a link will be provided upon acceptance of the manuscript). Genomic data is available at NCBI (accession number will be provided upon acceptance of the manuscript), and in the supplemental data file Table S1 and S2.

642 **References**

643

644 1. F. Fenner, I. D. Marshall, A comparison of the virulence for European rabbits
645 (Oryctolagus cuniculus) of strains of myxoma virus recovered in the field in
646 Australia, Europe and America. *The Journal of hygiene* **55**, 149-191 (1957).

647 2. S. R. Weiss, J. L. Leibowitz, Chapter 4 - Coronavirus Pathogenesis. *Advances
648 in Virus Research* **81**, 85-164 (2011).

649 3. S. L. Messenger, I. J. Molineux, J. J. Bull, Virulence evolution in a virus obeys
650 a trade-off. *Proceedings. Biological sciences* **266**, 397-404 (1999).

651 4. P. E. Turner, V. S. Cooper, R. E. Lenski, Tradeoff between Horizontal and
652 Vertical Modes of Transmission in Bacterial Plasmids. *Evolution* **52**, 315-329
653 (1998).

654 5. J. J. Bull, I. J. Molineux, W. R. Rice, Selection of Benevolence in a Host-Parasite
655 System. *Evolution* **45**, 875-882 (1991).

656 6. E. A. Herre, Population structure and the evolution of virulence in nematode
657 parasites of fig wasps. *Science* **259**, 1442-1445 (1993).

658 7. D. Ebert, Virulence and Local Adaptation of a Horizontally Transmitted
659 Parasite. *Science* **265**, 1084-1086 (1994).

660 8. M. Boots, Y. Haraguchi, The Evolution of Costly Resistance in Host-Parasite
661 Systems. *Am Nat* **153**, 359-370 (1999).

662 9. O. Restif, J. C. Koella, Shared control of epidemiological traits in a
663 coevolutionary model of host-parasite interactions. *Am Nat* **161**, 827-836 (2003).

664 10. M. van Baalen, Coevolution of recovery ability and virulence. *Proceedings.
665 Biological sciences* **265**, 317-325 (1998).

666 11. A. Mai-Prochnow *et al.*, 'Big things in small packages: the genetics of
667 filamentous phage and effects on fitness of their host'. *Fems Microbiol Rev*
668 10.1093/femsre/fuu007 (2015).

669 12. J. Bondy-Denomy, A. R. Davidson, When a Virus is not a Parasite: The
670 Beneficial Effects of Prophages on Bacterial Fitness. *J Microbiol* **52**, 235-242
671 (2014).

672 13. D. Refardt, Within-host competition determines reproductive success of
673 temperate bacteriophages. *Isme J* **5**, 1451-1460 (2011).

674 14. C. C. Wendling *et al.*, Tripartite species interaction: eukaryotic hosts suffer more
675 from phage susceptible than from phage resistant bacteria. *BMC Evol Biol* **17**
676 (2017).

677 15. E. A. Jouravleva *et al.*, The Vibrio cholerae mannose-sensitive hemagglutinin is
678 the receptor for a filamentous bacteriophage from V. cholerae O139. *Infect*
679 *Immun* **66**, 2535-2539 (1998).

680 16. J. J. Bull, C. S. Vegge, M. Schmerer, W. N. Chaudhry, B. R. Levin, Phenotypic
681 resistance and the dynamics of bacterial escape from phage control. *PLoS One*
682 **9**, e94690 (2014).

683 17. M. Leon, R. Bastias, Virulence reduction in bacteriophage resistant bacteria.
684 *Front Microbiol* **6**, 343 (2015).

685 18. T. Proft, E. N. Baker, Pili in Gram-negative and Gram-positive bacteria -
686 structure, assembly and their role in disease. *Cell Mol Life Sci* **66**, 613-635
687 (2009).

688 19. C. M. Chibani, R. Hertel, M. Hoppert, H. Liesegang, C. C. Wendling, Closely
689 Related Vibrio alginolyticus Strains Encode an Identical Repertoire of
690 Caudovirales-Like Regions and Filamentous Phages. *Viruses* **12** (2020).

691 20. S. Roux *et al.*, Cryptic inoviruses revealed as pervasive in bacteria and archaea
692 across Earth's biomes. *Nat Microbiol* **4**, 1895-1906 (2019).

693 21. T. J. Lerner, P. Model, The "steady state" of coliphage f1: DNA synthesis late in
694 infection. *Virology* **115**, 282-294 (1981).

695 22. I. D. Hay, T. Lithgow, Filamentous phages: masters of a microbial sharing
696 economy. *Embo Rep* **20** (2019).

697 23. M. K. Waldor, J. J. Mekalanos, Lysogenic conversion by a filamentous phage
698 encoding cholera toxin. *Science* **272**, 1910-1914 (1996).

699 24. M. D. Gonzalez, C. A. Lichtensteiger, R. Caughlan, E. R. Vimr, Conserved
700 filamentous prophage in Escherichia coli O18:K1:H7 and Yersinia pestis biovar
701 orientalis. *J Bacteriol* **184**, 6050-6055 (2002).

702 25. S. A. Rice *et al.*, The biofilm life cycle and virulence of Pseudomonas aeruginosa
703 are dependent on a filamentous prophage. *Isme J* **3**, 271-282 (2009).

704 26. P. R. Secor *et al.*, Filamentous Bacteriophage Promote Biofilm Assembly and
705 Function. *Cell Host Microbe* **18**, 549-559 (2015).

706 27. J. M. Sweere *et al*., Bacteriophage trigger antiviral immunity and prevent
707 clearance of bacterial infection. *Science* **363**, 1416-+ (2019).

708 28. C. C. Wendling, D. Refardt, A. R. Hall, Fitness benefits to bacteria of carrying
709 prophages and prophage-encoded antibiotic-resistance genes peak in different
710 environments. *Evolution* 10.1111/evo.14153 (2020).

711 29. I. Chouikha, L. Charrier, S. Filali, A. Derbise, E. Carniel, Insights into the
712 infective properties of Ypf Phi, the Yersinia pestis filamentous phage. *Virology*
713 **407**, 43-52 (2010).

714 30. A. Derbise *et al*., A horizontally acquired filamentous phage contributes to the
715 pathogenicity of the plague bacillus. *Mol Microbiol* **63**, 1145-1157 (2007).

716 31. L. M. Bobay, M. Touchon, E. P. C. Rocha, Pervasive domestication of defective
717 prophages by bacteria. *P Natl Acad Sci USA* **111**, 12127-12132 (2014).

718 32. B. M. Davis, K. E. Moyer, E. F. Boyd, M. K. Waldor, CTX prophages in
719 classical biotype Vibrio cholerae: functional phage genes but dysfunctional
720 phage genomes. *J Bacteriol* **182**, 6992-6998 (2000).

721 33. C. M. Chibani, O. Roth, H. Liesegang, C. C. Wendling, Genomic variation
722 among closely related Vibrio alginolyticus strains is located on mobile genetic
723 elements. *Bmc Genomics* **21**, 354 (2020).

724 34. C. C. Wendling, H. Goehlich, O. Roth, The structure of temperate phage-bacteria
725 infection networks changes with the phylogenetic distance of the host bacteria.
726 *Biol Lett* **14** (2018).

727 35. V. Poullain, S. Gandon, M. A. Brockhurst, A. Buckling, M. E. Hochberg, The
728 evolution of specificity in evolving and coevolving antagonistic interactions
729 between a bacteria and its phage. *Evolution* **62**, 1-11 (2008).

730 36. H. Goehlich, O. Roth, C. C. Wendling, Filamentous phages reduce bacterial
731 growth in low salinities. *Royal Society open science* **6**, 191669 (2019).

732 37. E. Harrison, D. Guymer, A. J. Spiers, S. Paterson, M. A. Brockhurst, Parallel
733 Compensatory Evolution Stabilizes Plasmids across the Parasitism-Mutualism
734 Continuum. *Curr Biol* **25**, 2034-2039 (2015).

735 38. R. E. Lenski, M. R. Rose, S. C. Simpson, S. C. Tadler, Long-Term Experimental
736 Evolution in Escherichia-Coli .1. Adaptation and Divergence during 2,000
737 Generations. *Am Nat* **138**, 1315-1341 (1991).

738 39. A. Bankevich *et al*., SPAdes: a new genome assembly algorithm and its
739 applications to single-cell sequencing. *J Comput Biol* **19**, 455-477 (2012).

40. H. Li, Minimap and miniasm: fast mapping and de novo assembly for noisy long sequences. *Bioinformatics* **32**, 2103-2110 (2016).

41. R. Vaser, I. Sovic, N. Nagarajan, M. Sikic, Fast and accurate de novo genome assembly from long uncorrected reads. *Genome Res* **27**, 737-746 (2017).

42. B. J. Walker *et al.*, Pilon: an integrated tool for comprehensive microbial variant detection and genome assembly improvement. *PLoS One* **9**, e112963 (2014).

43. C. S. Chin *et al.*, Nonhybrid, finished microbial genome assemblies from long-read SMRT sequencing data. *Nat Methods* **10**, 563-569 (2013).

44. G. Denisov *et al.*, Consensus generation and variant detection by Celera Assembler. *Bioinformatics* **24**, 1035-1040 (2008).

45. B. Langmead, S. L. Salzberg, Fast gapped-read alignment with Bowtie 2. *Nat Methods* **9**, 357-359 (2012).

46. D. E. Deatherage, J. E. Barrick, Identification of mutations in laboratory-evolved microbes from next-generation sequencing data using breseq. *Methods Mol Biol* **1151**, 165-188 (2014).

47. A. E. Darling, B. Mau, N. T. Perna, progressiveMauve: multiple genome alignment with gene gain, loss and rearrangement. *PLoS One* **5**, e11147 (2010).

48. M. J. Sullivan, N. K. Petty, S. A. Beatson, Easyfig: a genome comparison visualizer. *Bioinformatics* **27**, 1009-1010 (2011).

49. R. D. C. Team, R: A language and environment for statistical computing. R Foundation for Statistical Computing. *Vienna, Austria. ISBN 3-900051-07-0, URL* http://www.R-project.org/. (2011).

50. Y. Ram *et al.*, Predicting microbial growth in a mixed culture from growth curve data. *Proc Natl Acad Sci U S A* **116**, 14698-14707 (2019).